Influence of the inter-vehicle distance on the wake behind a three-dimensional body

Oumaïma Oussairan, Gilles Godard, Fabien Lefebvre, Carole Gobin, Benjamin Ouevreux, Béatrice Patte-Rouland, Georges Fokoua, Frédéric Murzyn, Emilien Varea

15th International Symposium on Particle Image Velocimetry – ISPIV 2023
June 19–21, 2023, San Diego, California, USA

Influence of the inter-vehicle distance on the wake behind a three-dimensional body

O. Oussairan[1*], G. Godard[1], F. Lefebvre[1], C. Gobin[1], B. Quevreux[1], B. Patte-Rouland[1], G. Fokoua[3], F. Murzyn[2], E. Varea [1]

[1] Normandy University, UNIROUEN, INSA Rouen, CNRS, CORIA, Rouen, 76000, France

[2] ESTACA Laval Campus, Department of Mechanical Engineering, Air Quality and Depollution Group, Rue Georges Charpak, Laval, 53000, France

[3] ESTACA Paris Saclay Campus, Department of Mechanical Engineering, Air Quality and Depollution Group, Avenue Paul Delouvrier, Saint Quentin en Yvelines, 78066, France

[*] oumaima.oussairan@coria.fr

Abstract

The flow behind a squareback and a fastback simplified car models are experimentally investigated. The influence of the inter-vehicle distance is highlighted. Ahmed bodies at a scale of 0.19 (Ahmed et al., 1984) are used in the experiments. The experiments are conducted in a closed-loop wind tunnel using a stereo particle image velocimetry at a fixed Reynolds number $Re = 4.9 \times 10^4$. The present work aims at studying and discussing the influence of a Following Vehicle (FV) and of the rear slant angle (φ) on the wake flow topology of the Leading Vehicle (LV). In this paper Four inter-vehicle distances are presented ranging from $0.93h_c$ to $3.70h_c$ with a step of $0.93h_c$, $h_c = 54$ mm being the width of the car model. For the leading vehicle, two rear slant angles are considered: squareback (0°) and fastback (25°). Mean properties of the flow and Reynolds stresses are presented. The transverse velocity measured behind the squareback car model in the presence of FV at 0.93 shows a bi-stability behavior. In order to obtain more characteristics about this unsteady wake, a LASER Doppler velocimetry in one dimensional is used.

1 Introduction

Related traffic air pollution is a major concern regarding the amount of emitted pollutants that can infiltrate the car passengers especially in urban areas. This leads to a deterioration of the air quality in the passenger compartment, thus the exposure of the occupants to pollution levels may exceed the recommended thresholds defined by the WHO (World Health Organization). Given that the pollutants emitted by a leading car are prone to infiltrate the compartment of the following car, it is crucial to consider the influence of wake on pollutant dispersion. Consequently, it becomes essential to enhance our understanding of the flow characteristics that emerge downstream of a car when a following vehicle is present.

The simplified geometry of car developed by Ahmed et al. (1984) know as Ahmed body is used in this study. Ahmed bodies are well-known in aerodynamic studies (Rodriguez et al., 2020; Essel et al., 2020; Grandemange et al., 2014; Leclerc, 2008) regarding their ability to reproduce similar physical structures that develop in the wake of road vehicles. Ahmed et al. (1984); Spohn and Gilliéron (2002); Gilliéron and Kourta (2011) and Lienhart and Becker (2003) presented a detailed description of the flow structures downstream Ahmed bodies. These structures and the associated drag force are highly dependent of the rear slant angle of the car 'φ'. In summary, three classes may be distinguished. For cars having a rear slant angle below $\sim 12.5^\circ$, the flow is two dimensional, it is fully attached on the rear angle and separates at the rear end. Two counter rotating vortices are developed behind the vertical base of the model in the close wake. The lower vortex is formed by the winding of the flow becoming beneath the model on its vertical base and the upper vortex is formed by the winding of the incoming flow to its vertical base. In addition, a toric shape is observed in the recirculation region. The drag is minimum for $\varphi = 12.5^\circ$. From $\sim 12.5^\circ < \varphi <\sim 30^\circ$, the drag increases to a maximum at $\varphi = 30^\circ$. In this case, the flow pattern is complex. It is partially separated from the rear slant angle. Longitudinal vortices appear, which take birth from the lateral sides of the vehicle.

The toric shape is still observed. For $\varphi >\sim 30^\circ$, the drag coefficient decreases and the behavior of the flow is similar to that observed for $\varphi <\sim 12.5^\circ$. However, the flow is fully detached on the rear slant and the longitudinal vortices do not longer exist. In this study, the Ahmed bodies used have a rear slant angles of $\varphi = 0^\circ$ and 25°.

To date, little attention has been focused on the interaction between two vehicles, the majority of the studies in the literature focus on the wake characteristics behind a single vehicle (Rodriguez et al., 2020; Barros, 2015; Leclerc, 2008; Grandemange et al., 2013; Thacker et al., 2013).

Essel et al. (2020) performed experimental particle image velocimetry (PIV) measurements between two in-line Ahmed bodies with a spacing distance of $0.75L_c$, $L_c = 196\,\text{mm}$ being the length of the model ($2.72h_c$, $h_c = 54\,\text{mm}$ being the width of the model). They demonstrate the wake characteristics between two in-line Ahmed bodies are influenced by two dominant motions: a downwash effect of the separated flow near the upper edge and a upwash of the flow near the lower rear edge. In their study, the upwash motion is dominant when the leading model has a squareback which results in a turbulence activity more enhanced in the upper shear layer. For a fastback car model, the downwash motion is stronger because of the inclined rear slant angle. As a result, the turbulence activity is larger in the lower shear layer.

An important characteristic may be added to the squareback is the unsteady wake. Indeed, the perfect symmetric of the set-up has sometimes direct influence on the wake. It leads to an unsteady wake behind the vehicle which shifts randomly between two preferred reflectional-positions. This is well-studied in the work of Grandemange et al. (2012). The bi-stability phenomenon downstream a squareback Ahmed body is also reported by Grandemange et al. (2013) and Volpe et al. (2015). In the works of Grandemange et al. (2013), the flow around a $1:4$ scale squareback Ahmed body at $Re = 9.2 \times 10^4$ was investigated using PIV measurements, and Hot-wire probes are used to obtain the unsteady characteristics of the flow. They showed that the bi-stability consists in a switch between two preferred positions at long time scales ($1000h_c/U_\infty$) associated with two equiprobable states of the base pressure gradient. They demonstrated that bi-stability is independent of the Reynolds number while it occurs only above a critical value of ground clearance. This latter affects the interaction between the top and bottom shear layers. Volpe et al. (2015) provide a detailed experimental information on the bi-stability phenomenon associated to a squareback Ahmed body. They showed that the time-scale of this phenomenon is of order of $800U_\infty/h_c$.

The objective of this paper is to better understand the interaction between two in-line Ahmed bodies and to investigate the bi-stability phenomenon.

2 Experimental facility and techniques

This work was conducted in the closed-loop wind tunnel of CORIA laboratory at the University of Rouen, France. The maximum velocity in the empty test section is of $16\,\text{m}\,\text{s}^{-1}$. The size of the associated test section is 0.4 m in high and wide and 2.5 m in long. The average turbulence intensity is less than 0.1%. The two transverse walls of the test section and the bottom plates are transparent, made of 8 mm thick glass, allowing optical measurements to be made. However, the upper plates are made of AU4G aluminum alloy. The bottom plate of the test section has an 80 mm hole at the end to allow insertion of the smoke generator tube. The test section is accessible from its side walls. The Ahmed body is used to generate wake topology of a typical ground car. The models are of 0.19 scale with respect to the generic one by the work of Ahmed et al. (1984). Indeed, the car models are 196 mm in length (L_c), 54 mm in height (h_c) and 73 mm in width (l_c). The car models are fixed by the 4 stilts of 15 mm in high and 4 mm in diameter upside down on the top plates of the test section as shown in the Figure 1. The dimensionless ground clearance is then $h_g^* = h_g/h_c = 15/54 = 0.28$. Considering the dimensions of the test section, the blockage effect is 2.7%, which falls below 5% that is considered as excessive rate. In that case, a correction should have been applied (West and Apelt, 1982). The first car model placed in the test section is called 'Leading Vehicle' (LV). A 'Following vehicle' (FV) is placed in four different positions away from the LV ranging from 50 mm to 200 mm with a step of 50 mm (Figure 1). The corresponding dimensionless inter-vehicle distances are $d^* = d/h_c = 0.93,\ 1.85,\ 2.78$ and 3.70. Beside the investigation of the inter-vehicle distance on the wake downstream the LV, another interest is given to the influence of the rear slant angle. To do this, two rear slant angles are considered for the LV. Thus, the first LV is a squareback car model, the rear slant angle is 0° and the second one is a fastback car model having a rear slant angle of 25°. The Figure 1 depicts the coordinate system adopted in this work. The x axis in the streamwise direction, whereas the y axis is directed in the vertical direction (normal to the ground) and the z axis is directed in order to complete the direct Cartesian system. It has its origin at the bottom of the rear face of the LV at the centerline of the test section. The coordinate system is also presented as (x^*, y^*, z^*), which represents the dimensionless distances with respect

to h_c. A rotation plate is mounted in order to center the position of the leading vehicle.

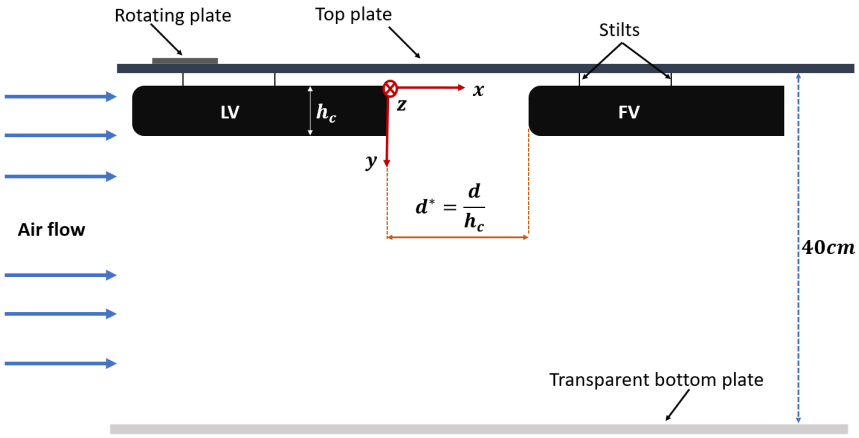

Figure 1: Side view of the car models placed in the test section with the coordinate system.

The wake topology between the two car models (LV and FV) is characterized using Stereo particle image velocimetry (SPIV). The system is composed of two cameras Phantom V2012 coupled with two Scheimpflug mounts and visible AF NIKKOR 80 – 220 f/2.8 and a ND-YAG LASER-Photonics DM150-532DH- cadenced at 20 kHz. The two cameras are placed on either side of the LASER sheet with an angle of 32.4°. Each camera acquires 3000 pairs of image at a rate of 600 Hz. The interrogation window size is 64×64 $pixels^2$ with an overlap of 50% which corresponds to a LASER sheet of 45 mm $\times$ 100 mm. However, the last LASER sheet which permits an overlap of 75%. The measurements are done in 4 planes: $z^* = 0,\ 0.31.\ 0.66$ and 0.90. The cameras and the optical instruments are mounted on a 3D-displacement system. The SPIV system permits the recording of the three components of the velocity field.

In addition to the SPIV measurements, Laser Doppler Anemometry (1D) measurements are undertaken downstream of the squareback Ahmed body (LV, $\varphi = 0°$) and the fastback Ahmed body (LV, $\varphi = 25°$) in order to assess the bi-stability phenomenon observed. The wavelength of LASER beams is 488 nm and the focal length is 500 mm. The number of frange is 35 and the inter-fringe spacing is 3.252 µm. The measurement volume is $0.1166 \times 0.1162 \times 1.549\,\text{mm}^3$. The acquisition is carried out in Burst mode in 300 s. The acquisition and the setting of the associated parameters are done on the BSA3 software of *Dantec*. The LDA measurements are performed in $x^* = 0.46,\ y^* = 0.50$ downstream the LV having a rear slant angle of 0° and in $x^* = 0.3,\ y^* = 0.50$ downstream the LV having a rear slant angle of 25°.

The incoming air flow velocity (U_∞) is determined to keep constant the ratio between the speed of the car and the velocity of the exhaust particles at the exit of the tailpipe (U_{tp}) in real-life conditions. As a consequence, the upstream velocity considered in the measurements is $U_\infty = 14.3\,\text{m s}^{-1}$ (Rodriguez, 2018). The velocity vector is defined as $\vec{u} = u\vec{e_x} + v\vec{e_y} + w\vec{e_z}$.

3 Results and discussion

3.1 Effect of the following vehicle

The mean flow downstream the LV having a squareback is shown in Figure 2. Figures 2(a) and 2(b) show the contours of the longitudinal and the vertical velocities between the two vehicles for the different inter-vehicle distances $d^* = 0.93$, $d^* = 1.85$, $d^* = 2.78$ and $d^* = 3.70$. The streamlines superimposed on the contours indicate the developing of two counter-rotating vortices in the near wake for each case. One can refer to Oussairan et al. (2023) for information on the positions of the centers of the vortices. For $d^* = 2.78$, the recirculation region which corresponds to the furthest point on zero-contour line (green dashed line), is equal to $1.50h_c$. This value is comparable to 1.53 reported in the study of Essel et al. (2020) (reduction of 2%). For $d^* = 1.85$, the plot shows that the recirculation bubble extends upstream the FV. Same observation for $d^* = 0.93$ where the recirculation bubble is dominant. For the highest inter-vehicle distance, the length of the recirculation is $1.26h_c$. For the two inter-vehicle distances $d^* = 2.78$ and 3.70 (Figure 2(b)), the

streamlines superimposed on the contours show an upwash. In addition, the streamlines coming from the upwash and the downwash deflect to the lower and the upper edges, respectively.

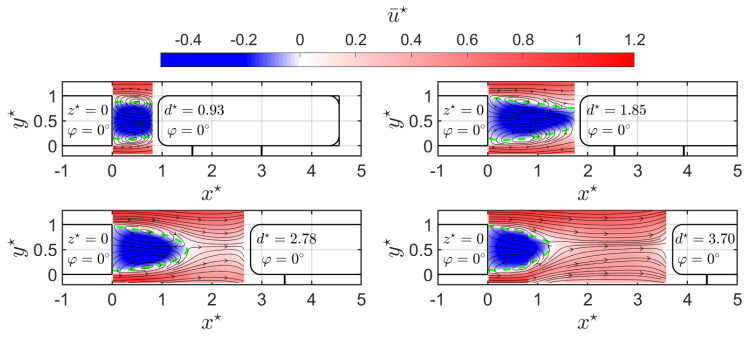

(a)

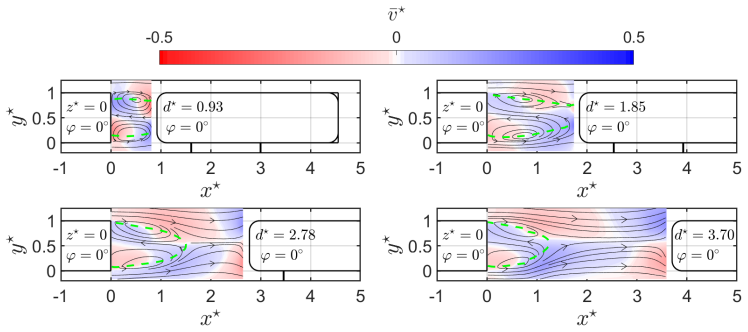

(b)

Figure 2: Contours of mean velocity in the plane $z^* = 0$, (a): $\bar{u}^*$ and (b): $\bar{v}^*$ downstream the squareback LV.

The contours of the longitudinal and vertical velocities downstream the LV having a fastback are presented in Figure 2. It is clear that the recirculation region is smaller than that observed downstream the squareback LV. It decreases by 65%, 61% and 55% in the case of $d^* = 1.85$, 2.78 and 3.70, respectively. The effect of the rear slant angle when the inter-vehicle distance is the smallest ($0.93h_c$) is negligible. In the study of Essel et al. (2020), the length of the recirculation region reported for $d^* = 2.72$ is equal to $1.23h_c$. This value is larger by 53% than of the present study ($0.58h_c$). This difference can be relied to the initial conditions of the experiments such that the Reynolds number. Indeed, in their study $Re = 1.7 \times 10^4$, while it is higher in the present study ($Re = 4.9 \times 10^4$). In addition, the Ahmed bodies are immersed in the turbulent boundary layer in that study ($\delta/h_c >> 1$) while in our study $\delta/h_c << 1$. The streamlines in Figure 3(b) when $d^* \geq 1.85$ show that the downwash from the upper edge is stronger than the upwash from beneath the LV. The streamlines coming from the upper edge deflect on either side of the FV which implies to a small recirculation region. The influence of the FV when the $d^* = 0.93$ is clearly seen. The downwash is weakly observed regarding the other cases. The upper vortex is having his center above $y^* = 0.5$, whereas it deviated to below $y^* = 0.5$ when $d^* \geq 2.78$.

The contours of the longitudinal (u'^{*2}), vertical (v'^{*2}) and shear ($u'^* v'^*$) Reynolds stresses downstream the LV having a squareback in the symmetry plane are presented in Figure 4. Behind the LV, the turbulence activity takes place in both upper and lower shear layers and towards to recirculation region. The results are in agreement with those found by Essel et al. (2020) and Grandemange et al. (2013). The vertical and shear Reynolds stresses exhibit an asymmetry shape. The turbulence activity is higher in the upper shear layer.

The contours of Reynolds stresses downstream the LV having a fastback show an asymmetry. The highest intensities are found in the lower shear layer. The asymmetry is attributed to the downwash effect from the upper edge. The results are in agreement with those reported in the studies Tunay et al. (2014); Grandemange et al. (2013); Rodriguez (2018).

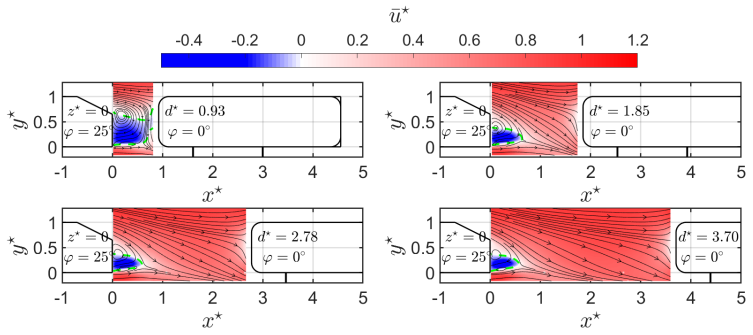

(a)

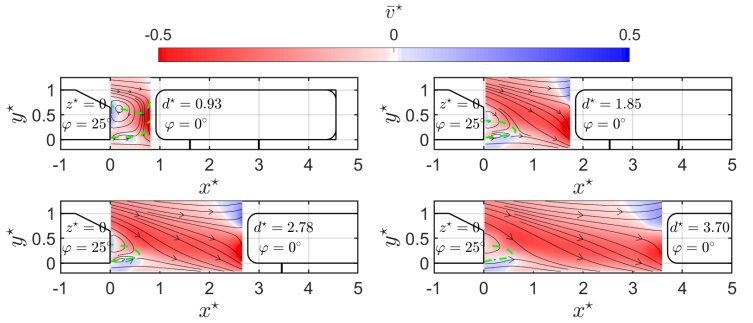

(b)

Figure 3: Contours of mean velocity in the plane $z^* = 0$, (a): $\bar{u}^*$ and (b): $\bar{v}^*$ downstream the fastback LV.

3.2 Dynamics of the flow, bi-stability

By placing the FV downstream of the LV $\varphi = 0^\circ$ at $d^* = 0.93$ (a distance less than the recirculation length $d^* = 1.40$), a so-called bi-stability behavior is observed. Indeed, we notice when processing the Stereo-PIV data that the average fields of the transverse velocity alternately record positive measurements for a certain time and then negative for another certain time (different from the first one). To further analyze the phenomenon, one dimensional LDA measurements are performed at the midpoint of the inter-vehicular distance $d^* = 0.93$. Figure 6 (left) shows an example of the time series of the transverse component of the velocity vector normalized by $U_\infty = 14.3\,\mathrm{m\,s^{-1}}$ for a duration of 300 s. It shows that the transverse velocity values shift from positive to negative values. During these 300 s, 18 phase switches were recorded between positive and negative positions. When analysing the time of each phase, we can notice that shift appears to be a random phenomenon and no natural frequency could be defined. This bi-stable behavior can be also seen in the associated probability density function associated, which reveals a bi-modal distribution with averaged velocity almost null (Figure 6, right).

In order to better understand this behavior, Figure 7 shows a rear view of the mean fields of the dimensionless transverse velocity and streamlines behind the squareback for $d^* = 0.93$ in the vertical planes $x^* = 0.48$ (in the core of the recirculation zone) and $x^* = 0.80$ (in the recirculation zone and upstream of the FV). Only, the positive half-width is presented. We observe the formation of the two contra-rotating vortices in $0 < z^* < 0.6$. For $x^* = 0.48$ the transverse velocity is higher ($\bar{w}^* = 0.23$) for $y^* = 0.6$. This value is lower in the case where $x^* = 0.8$ ($\bar{w}^* = 0.17$). It can be noticed that when the transverse velocity is higher, the vortices tend to move closer together. This creates a venturi effect that serves to disperse the flow outward. Thus, these vortices may explain the observation of random bi-stability created at this point.

These results are in agreement with those obtained by Grandemange et al. (2013) and Volpe et al. (2015) who well documented the bi-stability behavior resulting of dynamic switching between two symmetric configurations with respect to the central vertical plane. This explains that the symmetric flow topology results from the average of two asymmetric configurations. In the work of Grandemange et al. (2013), PIV velocity measurements are made downstream a $1/4$ reduced-scale Ahmed body with a ground clearance of $0.17h_c$. The flow generated in the wind tunnel has a Reynolds number equal to 9.2×10^4. They showed that at short time scale ($5\ h_c/U_\infty$) the wake exhibits weak coherent oscillations in the vertical and lateral directions. Similarly, in the work of Volpe et al. (2015), a low-frequency bi-stability phenomenon is detected downstream

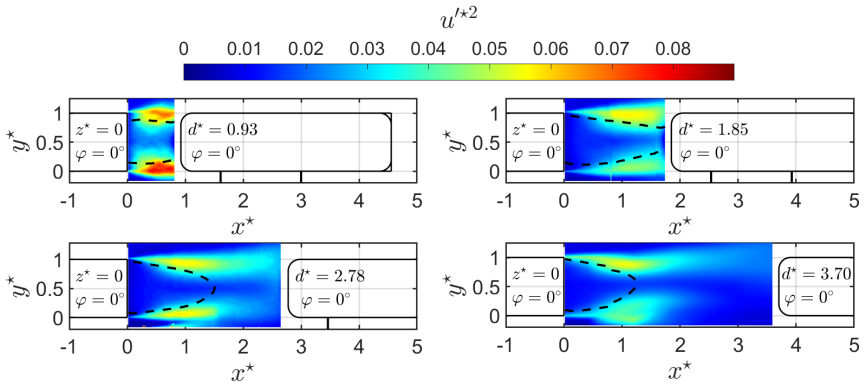

(a)

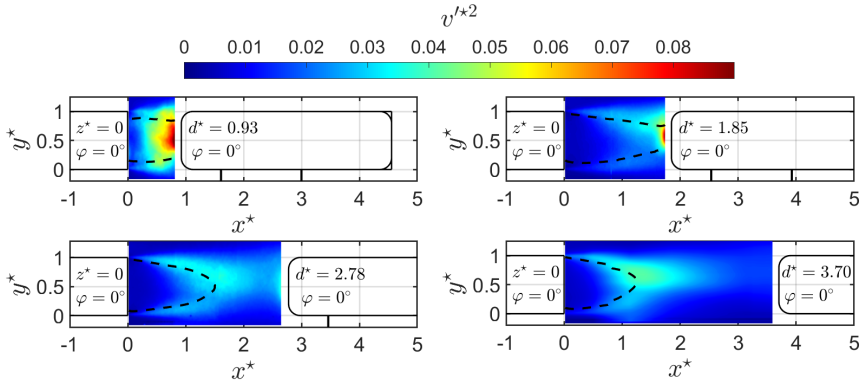

(b)

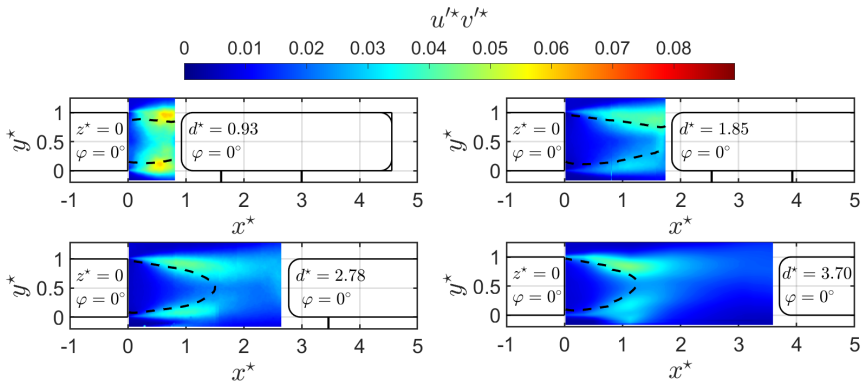

(c)

Figure 4: Contours of Reynolds stresses in the plane $z^* = 0$, (a): $u'^{\star 2}$, (b): $v'^{\star 2}$ and (c): $u'^\star v'^\star$ downstream the squareback LV.

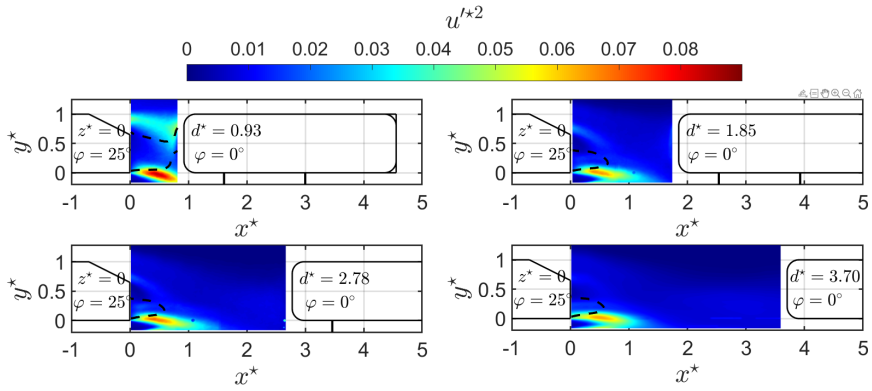

(a)

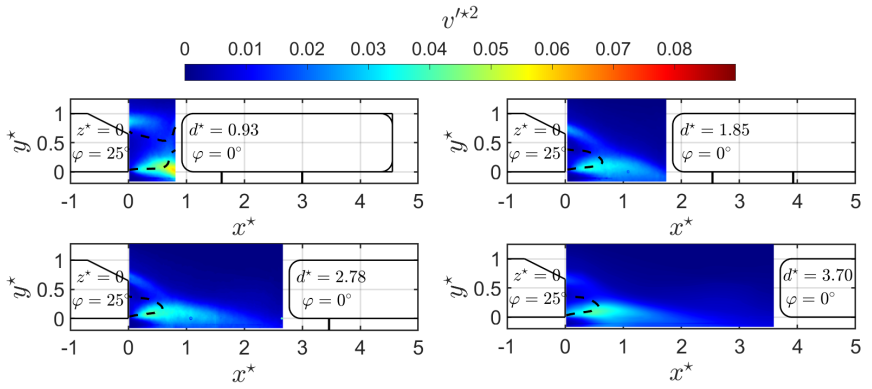

(b)

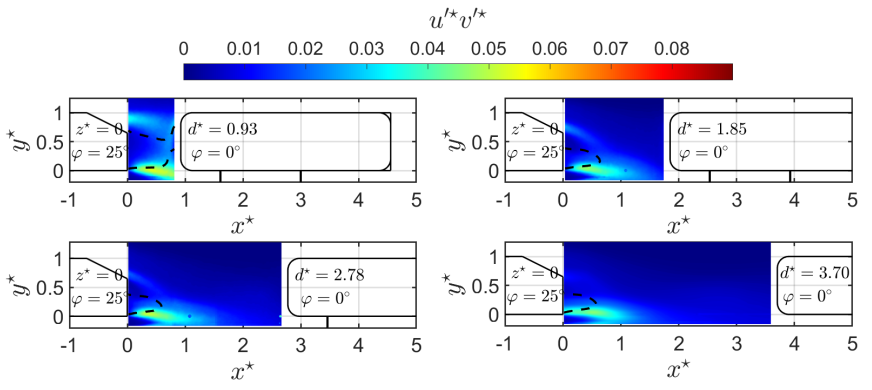

(c)

Figure 5: Contours of Reynolds stresses in the plane $z^* = 0$, (a): $u'^{\star 2}$, (b): $v'^{\star 2}$ and (c): $u'^\star v'^\star$ downstream the fastback LV.

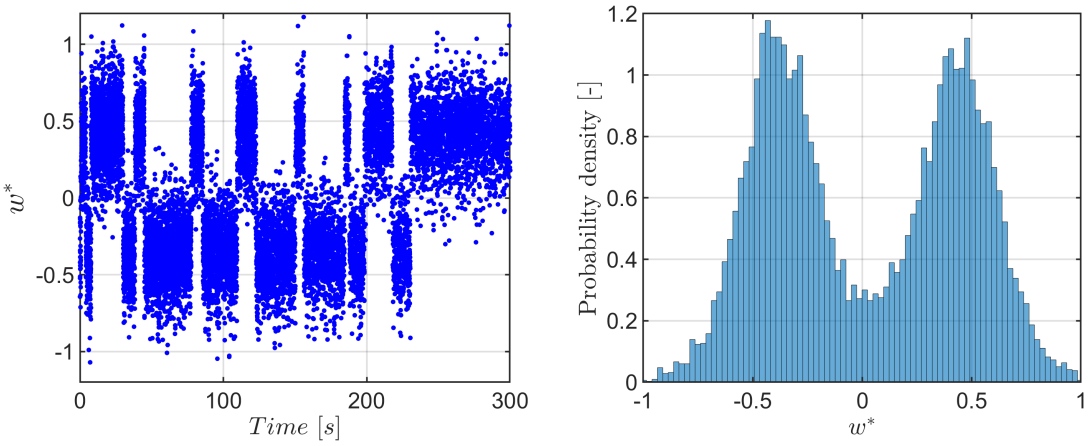

Figure 6: Time evolution and associated probability density distribution of the transverse velocity downstream the square model in the midpoint between the vehicles for $d^* = 0.93$.

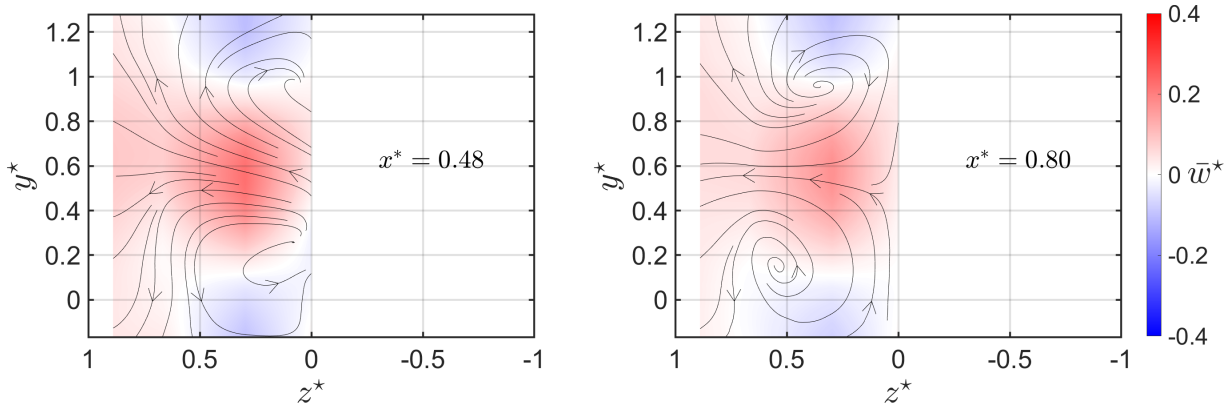

Figure 7: Rear view of the 2D mean maps of the dimensionless transverse velocity and the streamlines associated behind the LV $\varphi = 0°$ for $d^* = 0.93$ in the planes $x^* = 0.48$ and $x^* = 0.80$.

of a squareback Ahmed body in the vertical symmetric plane for measurement points in the recirculation zone ($Re = 5.2 \times 10^5$). We note that in these works, the bi-stability phenomenon is not only observed for the transverse velocity but also highlighted for the horizontal and vertical velocities. These results show that the wake presents a bi-stable behavior characterized by a random succession of switches between two respectively well defined configurations.

When increasing the inter-vehicle distance or changing the LV to the one having a fastback, the transverse velocity do not record any switching between positive and negative values even when placing the FV in the recirculation region (See Figure 8). This is in agreement with the average fields obtained with Stereo-PIV downstream the fastback LV, see Figure 9. The pattern of the flow is different from that seen behind the squareback LV. In this case, the flow tend to move outwards contrary to the case of LV having a squareback, see Figure 7. We can identify from the 9 two strong structures, one with positive values of transverse velocity values which is dominant and the other with negative ones. This behavior may rely on the strong downwash effect and to the vortices that have place on the frontal edges of the body who tend to direct the flow into the center of the vehicle.

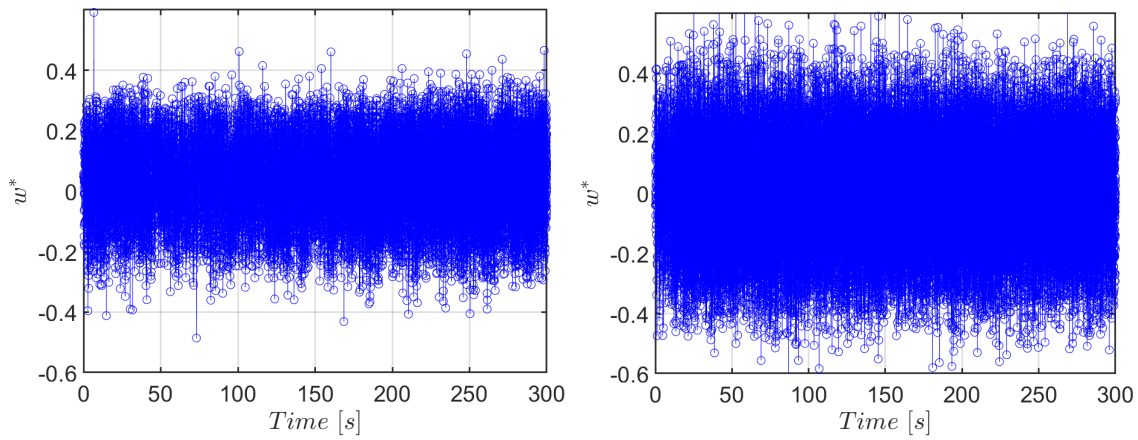

Figure 8: Time evolution of the transverse velocity in the midpoint between the vehicles for LV $\varphi = 0°$, $d^* = 1.85$ (left) and for LV $\varphi = 25°$, $d^* = 0.46$.

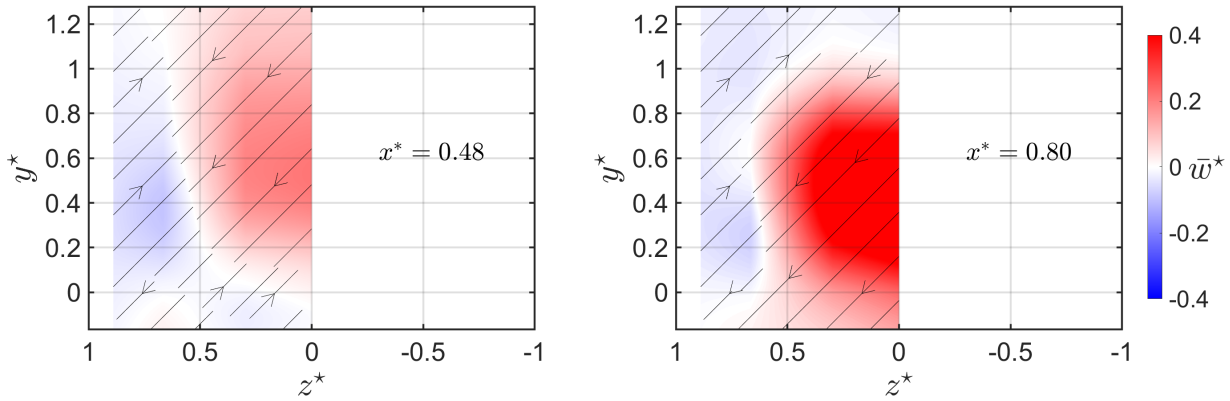

Figure 9: Rear view of the 2D mean maps of the dimensionless transverse velocity and the streamlines associated behind the LV $\varphi = 25°$ for $d^* = 0.93$ in the planes $x^* = 0.48$ and $x^* = 0.80$.

4 Conclusions

In this paper, an experimental investigation of the flow developping downstream two Ahmed bodies with two different rear slant angles ($\varphi = 0°$ and $25°$) considering the presence of the following vehicle has been carried out by means of Stereo PIV. The upstream velocity is $14.3\,\mathrm{m\,s^{-1}}$ leading to a Reynolds number of 49500 based on the height of the car model. Influence of inter-vehicle distances -d^*- and rear slant angles -φ- on Ahmed bodies wake flow are investigated. The analysis of the results showed that for $d^* = 2.78$ and $1.85h_c$, the influence of the FV is negligible on the mean and turbulent properties measured in the wake of the LV of $\varphi = 0°$ and $\varphi = 25°$, respectively. A specific flow topology which depicts an instantaneous loss of symmetry flow is observed when a leading vehicle is positioned in the recirculation zone of the squareback Ahmed body, $d^* = 0.93 < 1.40$. Therefore, even though the transverse velocity is null in average, the flow exhibits a bi-modal behavior.

Acknowledgements

The financial support of the University of Rouen and the Regional council of Normandy (France) are warmly acknowledged.

References

Ahmed SR, Ramm G, and Faltin G (1984) Some salient features of the time-averaged ground vehicle wake. *SAE Transactions* pages 473–503

Barros D (2015) *Wake and drag manipulation of a bluff body using fluidic forcing*. Ph.D. thesis. École Nationale Supérieure de Mécanique et d'Aérotechnique

Essel E, Das S, and Balachandar R (2020) Effects of rear angle on the turbulent wake flow between two in-line ahmed bodies. *Atmosphere* 11:328

Gilliéron P and Kourta A (2011) *Aérodynamique automobile pour l'environnement, le design et la sécurité*. Cépaduès

Grandemange M, Cadot O, and Gohlke M (2012) Reflectional symmetry breaking of the separated flow over three-dimensional bluff bodies. *Physical review E* 86:035302

Grandemange M, Gohlke M, and Cadot O (2013) Turbulent wake past a three-dimensional blunt body. part 1. global modes and bi-stability. *Journal of Fluid Mechanics* 722:51–84

Grandemange M, Gohlke M, and Cadot O (2014) Turbulent wake past a three-dimensional blunt body. part 2. experimental sensitivity analysis. *Journal of Fluid Mechanics* 752:439–461

Leclerc C (2008) *Réduction de la traînée d'un véhicule automobile simplifié à l'aide du contrôle actif par jet synthétique*. Ph.D. thesis

Lienhart H and Becker S (2003) Flow and turbulence structure in the wake of a simplified car model. *SAE transactions* pages 785–796

Oussairan O, Varea E, Fokoua G, Patte-Rouland B, and Murzyn F (2023) Interaction between two car models with application to pollutant dispersion. *Experimental Thermal and Fluid Science* 143:110815

Rodriguez R (2018) *Etude expérimentale de la dispersion de particules ultrafines dans le sillage de modèles simplifiés de véhicules automobiles*. Ph.D. thesis. École centrale de Nantes

Rodriguez R, Murzyn F, Mehel A, and Larrarte F (2020) Dispersion of ultrafine particles in the wake of car models: A wind tunnel study. *Journal of Wind Engineering and Industrial Aerodynamics* 198:104109

Spohn A and Gilliéron P (2002) Flow separations generated by a simplified geometry of an automotive vehicle. in *IUTAM Symposium: unsteady separated flows*. volume 1. Kluwer Academic

Thacker A, Aubrun S, Leroy A, and Devinant P (2013) Experimental characterization of flow unsteadiness in the centerline plane of an ahmed body rear slant. *Experiments in fluids* 54:1–16

Tunay T, Sahin B, and Ozbolat V (2014) Effects of rear slant angles on the flow characteristics of ahmed body. *Experimental Thermal and Fluid Science* 57:165–176

Volpe R, Devinant P, and Kourta A (2015) Experimental characterization of the unsteady natural wake of the full-scale square back ahmed body: flow bi-stability and spectral analysis. *Experiments in Fluids* 56:1–22

West G and Apelt C (1982) The effects of tunnel blockage and aspect ratio on the mean flow past a circular cylinder with reynolds numbers between 104 and 105. *Journal of Fluid mechanics* 114:361–377